

Critical exponents for crisis-induced intermittency

Celso Grebogi

Laboratory for Plasma and Fusion Energy Studies, University of Maryland, College Park, Maryland 20742

Edward Ott

*Laboratory for Plasma and Fusion Energy Studies and Departments of Electrical Engineering and Physics,
University of Maryland, College Park, Maryland 20742*

Filipe Romeiras*

Laboratory for Plasma and Fusion Energy Studies, University of Maryland, College Park, Maryland 20742

James A. Yorke

*Institute for Physical Science and Technology and Department of Mathematics,
University of Maryland, College Park, Maryland 20742*

(Received 1 July 1987)

We consider three types of changes that attractors can undergo as a system parameter is varied. The first type leads to the sudden destruction of a chaotic attractor. The second type leads to the sudden widening of a chaotic attractor. In the third type of change, which applies for many systems with symmetries, two (or more) chaotic attractors merge to form a single chaotic attractor and the merged attractor can be larger in phase-space extent than the union of the attractors before the change. All three of these types of changes are termed *crises* and are accompanied by a characteristic temporal behavior of orbits after the crisis. For the case where the chaotic attractor is destroyed, this characteristic behavior is the existence of chaotic transients. For the case where the chaotic attractor suddenly widens, the characteristic behavior is an intermittent bursting out of the phase-space region within which the attractor was confined before the crisis. For the case where the attractors suddenly merge, the characteristic behavior is an intermittent switching between behaviors characteristic of the attractors before merging. In all cases a time scale τ can be defined which quantifies the observed post-crisis behavior: for attractor destruction, τ is the average chaotic transient lifetime; for intermittent bursting, it is the mean time between bursts; for intermittent switching, it is the mean time between switches. The purpose of this paper is to examine the dependence of τ on a system parameter (call it p) as this parameter passes through its crisis value $p = p_c$. Our main result is that for an important class of systems the dependence of τ on p is $\tau \sim |p - p_c|^{-\gamma}$ for p close to p_c , and we develop a quantitative theory for the determination of the critical exponent γ . Illustrative numerical examples are given. In addition, applications to experimental situations, as well as generalizations to higher-dimensional cases, are discussed. Since the case of attractor destruction followed by chaotic transients has previously been illustrated with examples [C. Grebogi, E. Ott, and J. A. Yorke, *Phys. Rev. Lett.* **57**, 1284 (1986)], the numerical experiments reported in this paper will be for *crisis-induced intermittency* (i.e., intermittent bursting and switching).

I. INTRODUCTION

Crises^{1,2} are a common manifestation of chaotic dynamics for dissipative systems and have been seen in many experimental³ and numerical studies. In a crisis, one observes a sudden discontinuous change in a chaotic attractor as a system parameter is varied. The discontinuous changes are typically of three types: in the first a chaotic attractor is suddenly destroyed as the parameter passes through its critical crisis value; in the second the size of the chaotic attractor in phase space suddenly increases; in the third type (which can occur in systems with symmetries) two or more chaotic attractors merge to form one chaotic attractor. [The inverse of these pro-

cesses (i.e., the sudden creation, shrinking, or splitting of a chaotic attractor) occur as the parameter is varied in the other direction.]

For all three types of crisis there is an associated characteristic temporal dependence² of typical orbits for parameter values near the crisis. The characteristic temporal dependence can be quantified by a characteristic time² which we denote τ . The quantity τ is here taken to have the following meanings for the three different types of crisis.

(1) *Attractor destruction.* Let p denote the relevant system parameter, and let p_c denote the value of p at the crisis, with the destruction of the chaotic attractor occurring as p increases through p_c . Let p be slightly

larger than p_c , and consider orbits with initial conditions in the region of the basin of attraction of the attractor which existed for $p < p_c$. Such orbits will typically behave as a chaotic transient. That is, they are initially attracted to the phase-space region formerly occupied by the attractor for $p < p_c$; they then bounce around in this region in a chaotic fashion, which, for most purposes, is indistinguishable from the behavior of orbits on the chaotic attractor for $p < p_c$; finally, after behaving in this way for a possibly long time, they suddenly move away from the region of the former attractor (never to return) and approach some other attractor. The length of time an orbit spends on the remnant of the destroyed chaotic attractor depends sensitively on its initial condition, but, nevertheless, when many such orbits are considered, the length of the chaotic transient apparently has a well-defined average which tends to infinity as p approaches p_c . For example, one can choose some rectangular region in the basin and then calculate the chaotic transient lifetimes for many randomly chosen initial conditions in the rectangle. The average lifetime over these initial conditions is the same for different choices of the rectangle, as long as it lies in the interior of the former basin and p is close to p_c . We denote this average time τ .

(2) *Attractor widening.* As p increases through p_c the chaotic attractor suddenly widens. For p slightly larger than p_c , the orbit on the attractor typically spends long stretches of time in the old region to which the attractor was confined before the crisis ($p < p_c$). At the end of one of these long stretches, the orbit suddenly bursts out of the old region and bounces around in the new region made available to it at the crisis. It then returns to the old region for another long stretch, followed by another burst into the new region, and so on *ad infinitum*. The time between bursts (i.e., the length of the stretches in the old attractor region) has a more or less random appearance when tabulated. We define the characteristic time τ for this case to be the average over a long orbit of the time between bursts.

(3) *Attractor merging.* For $p < p_c$ there exist two chaotic attractors, each with its own basin of attraction. The two basins are separated by a basin boundary. As p is increased the two attractors enlarge and at the crisis ($p = p_c$) they both *simultaneously* touch the basin boundary separating their two basins. (At $p = p_c$ they also collide with saddle unstable orbits on the basin boundary.^{1,2}) For p slightly greater than p_c , an orbit will spend a long stretch of time in the region of one of the $p < p_c$ attractors. After such a time stretch, the orbit rather abruptly exits this region, and then spends a long stretch of time in the region of the other $p < p_c$ attractor, and so on. Thus, for $p > p_c$ there is one attractor on which the orbit intermittently switches between behaviors that, for a finite time, resemble orbits on the individual $p < p_c$ attractors. In this case the characteristic time τ is the average over a long orbit of the time between switches. (Two comments are in order. First, we have discussed the case where *two* attractors take part in the crisis; clearly more than two can conceivably be involved. Second, the fact that at $p = p_c$ both attractors *simultaneously* collide with the basin boundary is not to

be expected unless the system has some symmetry or other special property. One way this can occur is if the attractor of a map has m disjoint pieces, and the orbit cycles through them sequentially. In that case we can consider every m th iterate of the map. The resulting process then has m distinct attractors which can merge at p_c . In this case the system has the special feature that it is the m th iterate of a map.)

We use the term *crisis-induced intermittency* to describe the characteristic temporal behavior which occurs for the attractor-widening and attractor-merging crises.^{4,5} One may think of intermittency as meaning episodic switching between two (or more) sustained behaviors of different character. Thus we can schematically contrast the type of intermittency discussed by Pomeau and Manneville⁶ with what we discuss here, as follows. Pomeau-Manneville:

$$\begin{aligned} (\text{chaos}) \rightarrow \left[\begin{array}{c} \text{approximately} \\ \text{periodic} \end{array} \right] &\rightarrow (\text{chaos}) \\ &\rightarrow \left[\begin{array}{c} \text{approximately} \\ \text{periodic} \end{array} \right] \rightarrow \cdots \end{aligned}$$

Crisis-induced intermittency:

$$(\text{chaos})_1 \rightarrow (\text{chaos})_2 \rightarrow (\text{chaos})_1 \rightarrow (\text{chaos})_2 \rightarrow \cdots$$

For the case of intermittent bursting, we may take $(\text{chaos})_2$ to be a burst and $(\text{chaos})_1$ to be a chaotic orbit segment between the bursts. For the case of intermittent switching, $(\text{chaos})_1$ and $(\text{chaos})_2$ represent chaotic behaviors similar to those on the two attractors before the crisis.

Our main point in this paper is that for a large class of dynamical systems which exhibit crises, the dependence of τ on the system parameter is

$$\tau \sim (p - p_c)^{-\gamma}. \quad (1)$$

Furthermore, we shall develop a quantitative theory for the determination of the critical exponent γ for a broad class of low-dimensional systems. A number of examples for the case where the attractor is destroyed and replaced by a chaotic transient have been given by us in a previous preliminary publication.⁷ Thus we shall limit the examples given here to the case of crisis-induced intermittency.

As a first, and very simple, example² of crisis-induced intermittency, Fig. 1 shows time series for the quadratic map

$$x_{n+1} = p - x_n^2$$

for four values of p . The time series plotted is taken for every third iterate of the map for p values near the crisis which terminates the period-3 window.^{1,2} The initial condition is $x_0 = 0$. Figure 1(a) is just before the crisis, so that the orbit cycles through three chaotic bands. Since only the third iterate is plotted, the orbit in Fig. 1(a) is confined to one of those bands (actually the center band). Figures 1(b)–1(d) show orbits for p values above, the successively farther from, the crisis. Here we see that for long stretches the orbit remains in one band, but

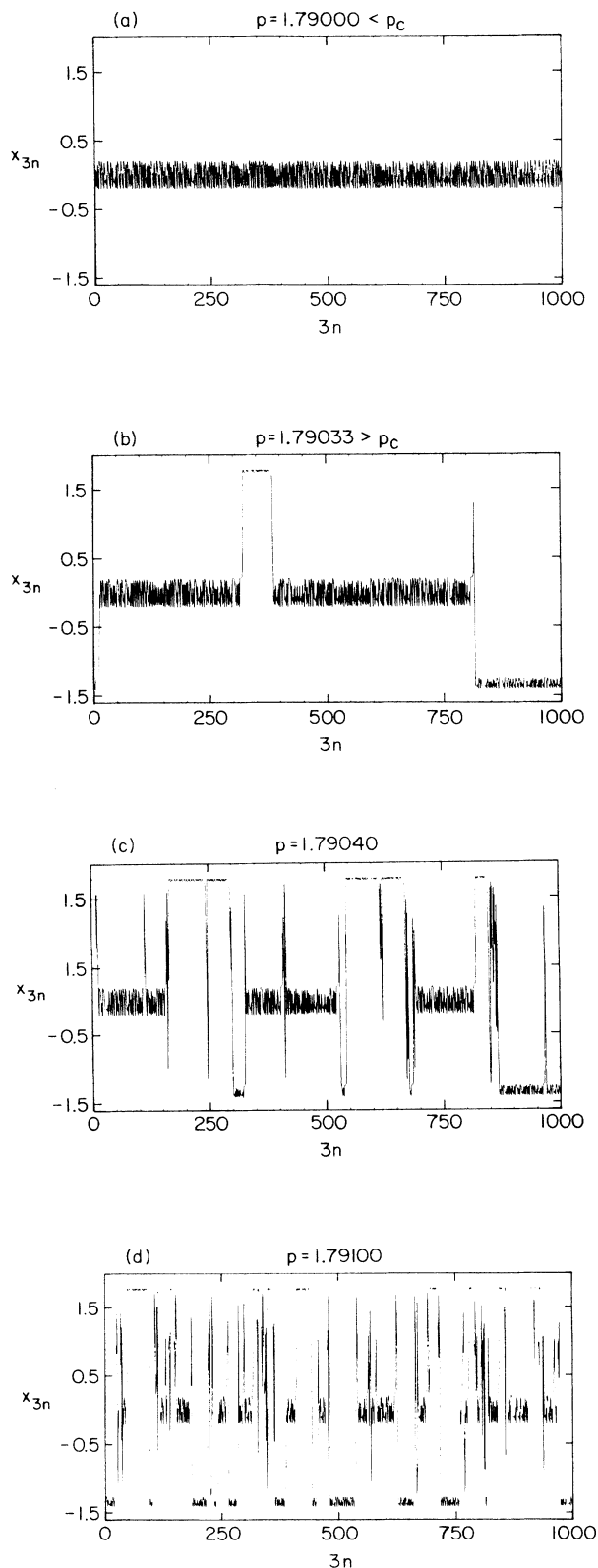


FIG. 1. Time series x_{3n} for the quadratic map near the crisis terminating the period-3 window $p < p_c$ (a), and $p > p_c$, (b), (c), and (d).

then occasionally bursts out of it and then returns to it or to one of the other two bands.

One of our main points is that larger values of the critical exponent γ make these phenomena easier to observe. From the numbers in the period-3 window example [$p = 1.79000, 1.79033, 1.79040, 1.79100$ for Figs. 1(a)–1(d)], we see that the range of the parameter involved $1.791 - 1.790 = 0.001$ is small compared to the size of the period-3 window, which covers $1.75 < p \leq 1.79$. Thus, for this case, the crisis-induced intermittency phenomenon only exists over a comparatively small range of the parameter. As we shall see in our subsequent numerical examples, this need not be the case when γ is larger. This can be easily seen from the following example. Say that $\tau = C(p - p_c)^{-\gamma}$, and consider two cases, one with $\gamma = \frac{1}{2}$ and the other with $\gamma = 2$, and take $C = 1$ for both cases. [One-dimensional maps with quadratic extrema always yield $\gamma = \frac{1}{2}$ (e.g., the period-3 window crisis of Fig. 1).] For this hypothetical case, we have that the range of p with $\tau > 100$ is $0 < (p - p_c) < 0.1$ for $\gamma = 2$ and $0 < (p - p_c) < 0.0001$ for $\gamma = \frac{1}{2}$.

In Sec. II we first summarize the results of our theory for the determination of the critical exponent γ for a wide class of two-dimensional maps. The theory also applies to many continuous time systems whose Poincaré surface of section yields a two-dimensional map. We then illustrate the application of the theory with three physically interesting examples: the Ikeda map (which represents a model of a laser cavity system); the sinusoidally forced damped pendulum (this equation also describes the dynamics of simple Josephson-junction circuits and charge-density waves in solids); and the sinusoidally driven symmetric double-well system (the crisis in this case has been previously investigated numerically in Ref. 8). We then discuss the application of these ideas to the determination of exponents for the mergings of chaotic bands which occurs in period-doubling cascades. A finite Jacobian, universal correction to the one-dimensional result ($\gamma = \frac{1}{2}$) is obtained near the Feigenbaum point.

Section II also provides some discussion on how to apply the theory in experimental situations. The problem is that our formulas for γ are in terms of the eigenvalues of certain unstable orbits. While these can be determined from computer models of the system, it is clearly preferable to do this directly from experimental data, thus negating the need for a mathematical model. Methods for doing this are discussed.

Section III derives the theoretical results for γ quoted in Sec. II. (Some of this material has previously appeared in a preliminary form in Ref. 7.) We emphasize that, although our examples in Sec. II are all for crisis-induced intermittency, this theory applies equally to the case of chaotic transients following the destruction of a chaotic attractor by a crisis.⁷

Section IV discusses extensions of the theory of Sec. III to other situations. In particular, higher-dimensional situations (Sec. IV A) and the effect of fixed points in three-dimensional autonomous flows (Sec. IV B) are considered. Both effects lead to enhanced values of γ . It is

speculated, on the basis of this analysis, that chaotic bursting and chaotic transient phenomena are likely to be prominent in situations where higher-dimensional attractors occur (in the sense that they will occupy a relatively large volume in the parameter space).

Remark. Equation (1) does not apply to all crises. In particular, in Ref. 9 we have investigated a type of crisis which occurs as a result of a coalescence of two unstable periodic orbits (the “unstable-unstable pair bifurcation”). For this type of crisis

$$\tau \sim \exp[\kappa(p - p_c)^{-1/2}],$$

where κ is a constant. Comparing this expression for τ with (1), we may regard the critical exponent as being infinite ($\gamma = \infty$) for unstable-unstable pair bifurcation crises, since τ approaches infinity as p approaches p_c faster than any power of $(p - p_c)^{-1}$. We emphasize, however, that, from our studies of chaotic transients, in practice we find that instances where (1) applies seem to be the most common situation by far. (Indeed this is reasonable, since we expect the hypotheses adopted in our analyses of Secs. III and IV to be satisfied in many cases.)

II. THEORETICAL RESULTS FOR TWO-DIMENSIONAL MAPS AND EXAMPLES

A. Summary of results from Sec. III

In Sec. III we derive formulas for the critical exponent for a broad class of two-dimensional maps. In particular, we consider two-dimensional maps for which the crisis is due to a tangency of the stable manifold of an unstable periodic orbit with the unstable manifold of another or the same periodic orbit. These types of crises appear to be the *only* kinds of crises which can occur for invertible two-dimensional map systems that are strictly dissipative (i.e., magnitude of Jacobian determinant less than 1 everywhere) and they are ubiquitous features in such commonly studied nonlinear systems as the forced damped pendulum (or Josephson junction), the forced Duffing equation, the Hénon map, and many others.

At the crisis the tangency can occur in two possible ways.

(i) *Heteroclinic tangency.* In this case, the stable manifold of an unstable periodic orbit (B) is tangent to the unstable manifold of an unstable periodic orbit (A) on the attractor, as in Fig. 2(a).

(ii) *Homoclinic tangency.* In this case, the stable and unstable manifolds of an unstable periodic orbit (B) are tangent, as in Fig. 2(b).

In the derivation (given in Sec. III) of our formulas for γ , it is assumed that the tangencies occurring in Figs. 2 are of the quadratic type. In both cases, the chaotic attractor is the closure of one of the branches of the unstable manifold of B (for Fig. 2, the branch leaving B going toward the right). For the case of Fig. 2(a), the chaotic attractor is also the closure of the unstable manifold of A .

We show in Sec. III that the critical exponent γ obeys two distinct laws depending on the type of tangency the

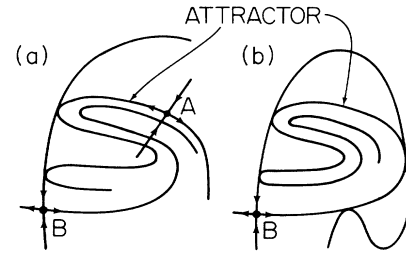


FIG. 2. (a) Schematic illustration of heteroclinic tangencies of the stable manifold of the unstable periodic orbit B and the unstable manifold of the unstable periodic orbit A . (For simplicity we take the periods of A and B to be 1.) (b) Schematic illustration of homoclinic tangencies of the stable and unstable manifolds of the unstable periodic orbit B .

system exhibits at the crisis. In the case of a heteroclinic crisis, we have

$$\gamma = \frac{1}{2} + (\ln |\alpha_1|) / |\ln |\alpha_2||, \quad (2)$$

where α_1 and α_2 are the expanding ($|\alpha_1| > 1$) and contracting ($|\alpha_2| < 1$) eigenvalues, respectively, of the periodic orbit A in Fig. 2(a). In the case of a homoclinic crisis, we have

$$\gamma = (\ln |\beta_2|) / (\ln |\beta_1 \beta_2|^2), \quad (3)$$

where β_1 and β_2 are the expanding and contracting eigenvalues of the periodic orbit B in Fig. 2(b). In the limit of strong contraction ($\alpha_2, \beta_2 \rightarrow 0$), Eqs. (2) and (3) yield $\gamma = \frac{1}{2}$, the result for a one-dimensional map with a quadratic maximum.

In Figs. 2 we have schematically shown the simple case where A and B are fixed points; for the case where A and B are periodic orbits similar diagrams can be drawn. In this case $\alpha_1, \alpha_2, \beta_1$, and β_2 are the eigenvalues of the n -times iterated map, where n is the orbit period. For Fig. 2(a) a question that may arise is whether the periods of A and B are related. For the case where B is on a basin boundary (as for the attractor-destroying and attractor-merging crises), we show in the Appendix that, in fact, the periods of A and B must be identical. [We were originally led to suspect that this might be the case by our numerical study of the Ikeda map (Sec. II C), where we found a case for which both A and B are period-5 orbits.]

Several remarks are now in order.

(1) In the case of a boundary crisis^{1,2} (i.e., where the attractor collides with its basin boundary) the closure of the stable manifold of B is also the boundary of the basin of attraction of the attractor. [The case of boundary crises applies when the crisis either causes two attractors to merge (cf. Secs. II D–II F) or destroys the attractor.]

(2) If the system is not strictly dissipative, then crises need not occur only as a result of stable and unstable manifold tangencies. In particular, there is a possibility of the unstable-unstable pair bifurcation crisis⁹ (cf. remarks at the end of Sec. I). This type of bifurcation can-

not occur, however, if the Jacobian determinant has magnitude less than one, since this bifurcation involves the coalescence of a saddle periodic orbit with a repelling period orbit, and repellers are ruled out in the strictly contracting case.

(3) For strictly dissipative maps $|\alpha_1\alpha_2| < 1$, and hence γ from Eq. (2) lies in the range $\frac{1}{2} \leq \gamma \leq \frac{3}{2}$ with $\gamma \rightarrow \frac{3}{2}$ as $|J| \rightarrow 1$. For the homoclinic case $\gamma \rightarrow \infty$ as $|J| \rightarrow 1$ [cf. Eq. (3)].

(4) The assumption of a quadratic tangency is appropriate (generic) for maps which are C^2 . We note, however, that Poincaré maps resulting from flows need not be of this type.

(5) In general, three-dimensional flows (e.g., a system of three autonomous first-order ordinary differential equations) that are sufficiently smooth, and for which the time between crossings of the Poincaré surface of section has an upper bound, generically result in invertible C^2 maps (assuming the vector field is nowhere tangent to the chosen surface of section). For example, for periodically forced systems, one can sample the orbit at the forcing period, and the time between surface piercings is clearly a constant (the forcing period). For other cases such as the Lorenz equations (cf. Sec. IV B), however, the orbit can pass arbitrarily close to a fixed point in the flow, and, when it does so, it spends a long time near this point. Thus the time between section crossings can be arbitrarily long. This results in the well-known cusp in the Lorenz return map.

(6) As p is varied close to the tangency ($p = p_c$), very small parameter windows exist where periodic attractors (of possibly high period) occur ("Newhouse sinks"). In our computations of τ from orbit data, we picked many values of p near p_c , but apparently never fell in one of these narrow windows. The result, Eq. (1), is to be understood as excluding p values in such windows.

(7) For the case of a boundary crisis, at $p = p_c$ the attractor touches the basin boundary at its point of tangency with the stable manifold of B . Thus an entire ϵ neighborhood of every point on the attractor (in particular, the tangency point) does not tend to the attractor. Hence, by the definition of an attractor used by some authors, what we are here calling the "attractor" is not an attractor at $p = p_c$.

B. Experimental determination of eigenvalues

In an experimental situation the characteristic time τ can, in principle, be measured as a function of a system parameter in the neighborhood of the crisis. By analyzing the results of such measurements, the critical exponent γ can be determined. In order to compare this experimental γ with the theoretical prediction given in Eqs. (2) and (3), it is necessary to know the eigenvalues, α_1 and α_2 for Eq. (2) or β_1 and β_2 for Eq. (3). Here we briefly discuss how these eigenvalues might be determined *directly* from experimental data. We emphasize that in the following discussion we assume that a mathematical model of the experimental system is unavailable. (If one were known it could be used to determine the eigenvalues.)

First consider the case of the homoclinic crisis, Eq. (3). In this case we require knowledge of β_1 and β_2 . Consider the case where p is just slightly larger than p_c (i.e., $r \equiv p - p_c \ll 1$ and $r > 0$), and ask what happens near the initiation of a burst or switch (for crisis-induced intermittency), or, equivalently, what happens at the end of a chaotic transient (for the case where the crisis destroys the attractor). For $p > p_c$ ($r > 0$) the unstable manifold of B in Fig. 2(b) pokes over to the other side of the stable manifold of B . An orbit may be pictured as bouncing around for a long time on the unstable manifold of B in the region of the attractor before the crisis. After a while, it may land on the portion of the unstable manifold of B which has poked over to the other side of the stable manifold of B (point 1 in Fig. 3). Since we consider r small, the location of the orbit at this time is near the stable manifold of B . On further iteration, this orbit point is attracted toward B along its stable manifold (1 \rightarrow 2 \rightarrow 3 \rightarrow 4 in Fig. 3) and then repelled from B along the segment of its unstable manifold which points away from the former region of the attractor. By examining the locations of the orbit points (the dots in the figure) one can deduce an estimated location of B (denoted by an x in the figure) and the orientation of the stable and unstable manifolds of B . Determining the distances from the estimated location of B to successive orbit locations (e.g., l_1, l_2, l_3, l_4 in the figure), then yields estimates of β_1 and β_2 , e.g.,

$$\beta_1 \cong (l_3/l_4), \quad (4)$$

$$\beta_2 \cong (l_2/l_1). \quad (5)$$

If B is a periodic orbit of period m , rather than a fixed point of the map (as assumed in the above), then Fig. 3 should be regarded as applying to the m th iterate of the map, and B is one of the m components of the periodic orbit.

Now we consider the case of the heteroclinic crisis, Eq. (2). Here we need to gain a knowledge of the eigenvalues α_1 and α_2 of the unstable orbit A on the attractor. For r small, an orbit point which crosses over to the other side of the stable manifold of B (as in Fig. 3) does so by closely following the unstable manifold of A .

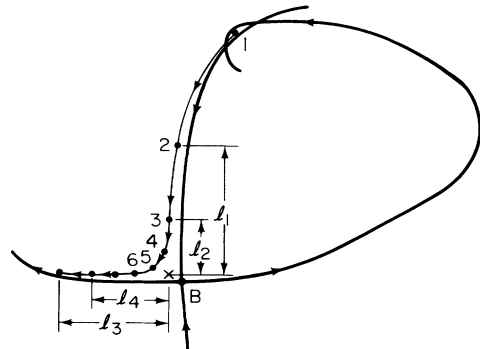


FIG. 3. Schematic of the orbit as a burst is initiated. The x denotes the "estimated" location of B .

Thus if one looks at the immediate preiterates of such a point, they must pass close to A . By examining such preiterates the location and period of A can be determined. If r is sufficiently small, the orbit may pass close enough to A that the eigenvalues α_1 and α_2 can also be determined (the orbit near A will be like that illustrated for B in Fig. 3). Even if this is not the case, all is not lost. In particular, during the long time the orbit spends before leaving the region of the attractor by crossing over the stable manifold of B , it will come close to A many times, and some of these close approaches will be very much closer than the one that ultimately lets the orbit leave. By examining the data for the closest approach, a string of orbit points can be determined which can yield a good estimate of α_1 and α_2 via the construction illustrated in Fig. 3 for B .

When determining γ appearing in the formula $\tau \cong C |p - p_c|^{-\gamma}$, there are three unknown constants (C , p_c , and γ), and one might initially expect to be forced to measure τ for at least three values of p to find γ . Thus it is interesting to note that the experimental procedure for determining the $\alpha_{1,2}$ and $\beta_{1,2}$ eigenvalues outlined above in conjunction with Eqs. (2) and (3) yields γ and hence the dependence of τ on a parameter via measurements performed at a *single* value of the parameter. Furthermore, since no parameter is varied in this determination, the exponent is typically independent of which parameter is varied.

In Secs. II C–II F we present examples illustrating the utility of Eqs. (2) and (3). Example 1 illustrates a heteroclinic crisis where Eq. (2) applies. Examples 2 and 3 illustrate homoclinic crises [Eq. (3)].

C. Example 1: The Ikeda map

The Ikeda map is given by

$$z_{n+1} = A + Bz_n \exp[i\kappa - ip/(1 + |z_n|^2)], \quad (6)$$

where $z = x + iy$ is a complex number; $x = \text{Re}(z)$, $y = \text{Im}(z)$. This map models the behavior of a laser system (cf. Fig. 4 and figure caption). For our purposes, we regard (6) as a real two-dimensional map in the variables (x_n, y_n) . We investigate (6) for $A = 0.85$, $B = 0.9$, $\kappa = 0.4$, and vary p in a range about the crisis value, $p_c = 7.268\,848\,94 \dots$. Figure 5 shows y_n versus n for several values of the parameter p (successive y_n are joined by straight lines). In Fig. 5(a) p is less than p_c , while Figs. 5(b)–5(d) show results for successively larger p values past p_c . Intermittent bursting is evident past p_c , and the time between bursts is seen to decrease with increasing $p - p_c$. Figure 6(a) shows the chaotic attractor for a case with $p < p_c$, while Fig. 6(b) shows that the attractor has greatly widened for $p > p_c$. Note that the additional regions visited in Fig. 6(b) [as compared to Fig. 6(a)] are sparse in orbit points; this reflects the relatively small fraction of time spent by the orbit in executing bursts. Figure 6(a) also shows the locations of two period-5 orbits, $B_1 \rightarrow B_2 \rightarrow B_3 \rightarrow B_4 \rightarrow B_5 \rightarrow B_1 \rightarrow \dots$, and $A_1 \rightarrow A_2 \rightarrow A_3 \rightarrow A_4 \rightarrow A_5 \rightarrow A_1 \rightarrow \dots$. Orbit B is the unstable orbit whose stable manifold the attractor

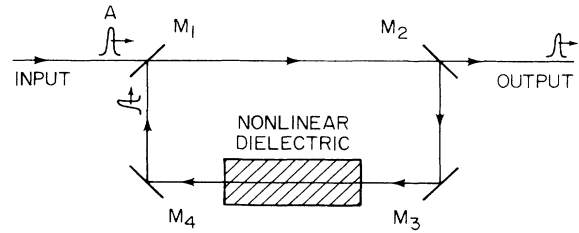


FIG. 4. The Ikeda map can be viewed as arising from a string of light pulses of amplitude A entering at the partially transmitting mirror M_1 . The time interval between the pulses is adjusted to the round-trip travel time in the system. Let $|z_n|$ be the amplitude and angle (z_n) be the phase of the n th pulse just to the right of mirror M_1 . Then the terms in (6) have the following meaning: $(1-B)$ is the fraction of energy in a pulse transmitted or absorbed in the four reflections from M_1 , M_2 , M_3 , and M_4 ; κ is the round-trip phase shift that would be experienced by the pulse in the absence of the nonlinear medium; $-p/(1 + |z_n|^2)$ is the phase shift due to the presence of the nonlinear medium.

collides with as the crisis is initiated (Fig. 2). We determined B by examining time series for p slightly greater than p_c (as discussed in Sec. II B and Fig. 3). We then calculated the eigenvalues of the fifth iterate of the map at B_1 (the same eigenvalues apply at B_2 to B_5). Using these in the formula for homoclinic crises, Eq. (3), we obtained a value for the exponent which was in clear disagreement with our data for τ versus $(p - p_c)$. Hence we are led to consider the possibility of a heteroclinic crisis. We thus searched for an orbit A on the attractor whose unstable manifold can become tangent to the stable manifold of B at $p = p_c$. Such an orbit is expected to lie on the outer envelope of the attractor. To find A we utilized the interactive capabilities of a personal computer with successive (x, y) orbit points plotted on the screen.¹⁰ Starting with an initial condition on the outer edge of the attractor, we iterated the map five times and observed the location of the fifth iterate in relation to the starting point. If there exists a fixed point for the fifth iterate of the map in that neighborhood, the starting point and its fifth iterate should lie roughly along the same branch of the unstable manifold of this orbit. Thus, by moving the starting point away from its fifth iterate and along the outer edge of the attractor, we were able to find one of the components of the unstable periodic orbit A . Given approximate positions for A and B , Newton's method provides more precise values. Having determined A we then used Eq. (2) to obtain γ . The results from the numerical experiments shown in Fig. 7 (dots) are in excellent agreement with the theoretical prediction (straight line). The calculations of the average lifetimes (the dots on the figure) from the data of the numerical experiments were done as follows. We know that, at the beginning of a burst, the orbit leaves the vicinity of the $p < p_c$ attractor by shooting out along the unstable manifold of B . Say we look at the orbit near B_2 at the beginning of a burst. We see that every

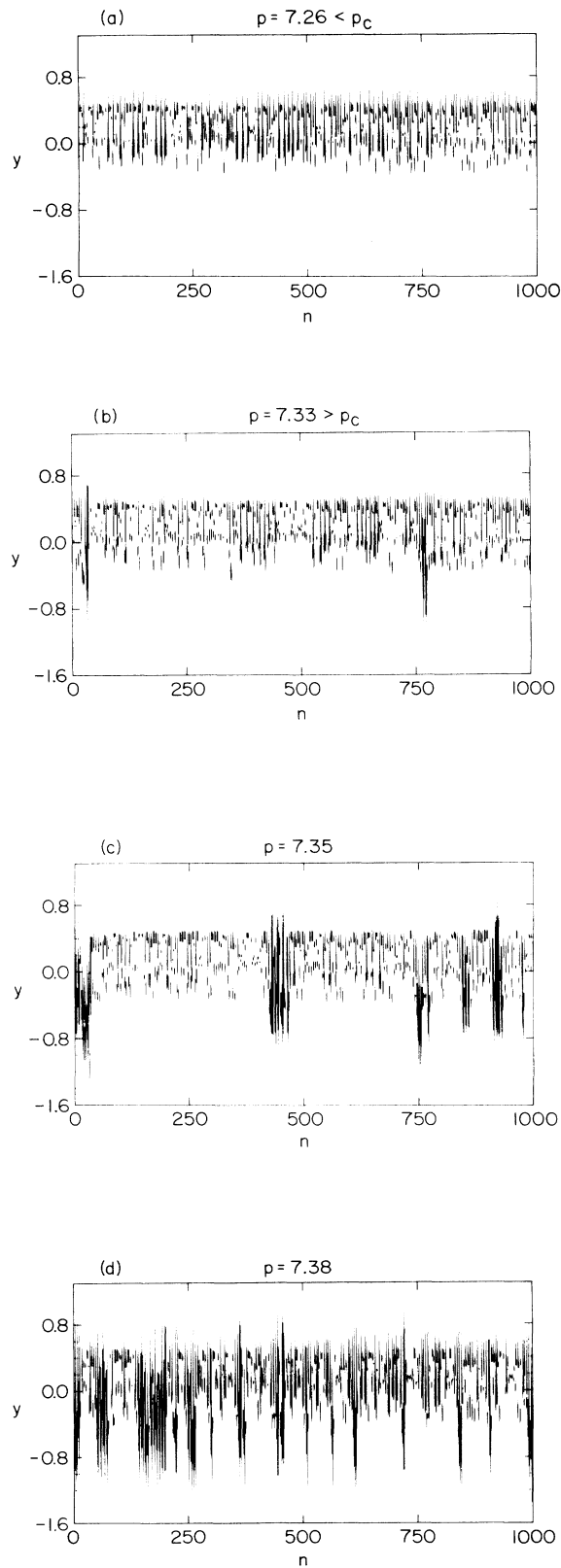


FIG. 5. $y = \text{Im}(z)$ vs n for four different values of p .

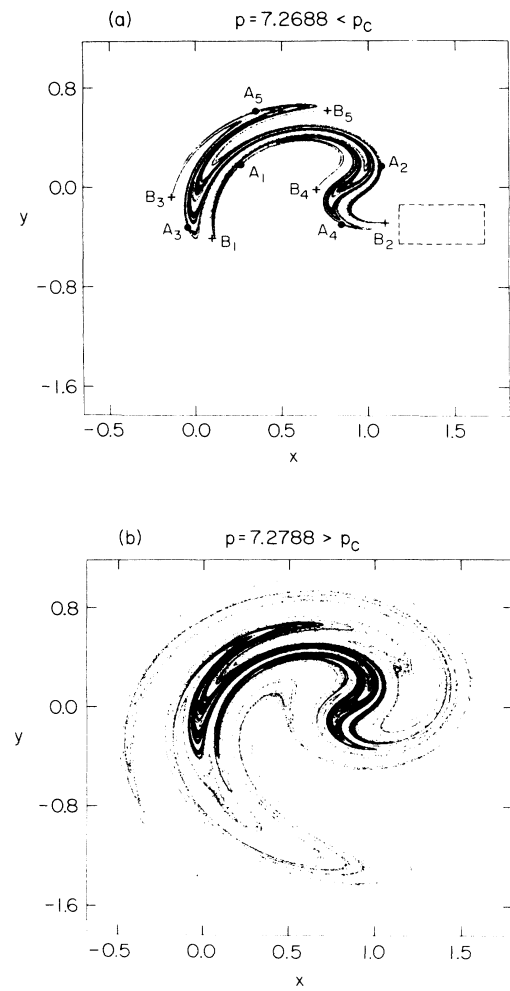


FIG. 6. Attractors before (a) and after (b) the crisis.

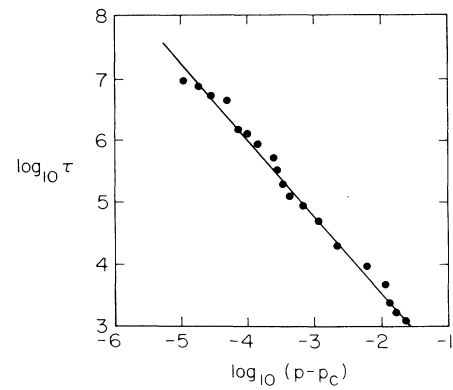


FIG. 7. $\log_{10} \tau$ vs $\log_{10}(p - p_c)$. The eigenvalues are $\alpha_1^{1/5} = 1.7972$ and $\alpha_2^{1/5} = 0.4507$. The theoretical exponent from Eq. (2) is $\gamma = 1.236$. The solid line is $\tau = 12.14(p - p_c)^{-1.236}$.

fifth orbit point approaches B_2 moving upward (along the stable manifold of B) and then shoots out toward the right. Thus our numerical criterion for the initiation of a burst is that an orbit point falls in some suitably chosen region to the right of B_2 [such a region is the dashed rectangle shown in Fig. 6(a)]. By this means we can automate the accurate computer determination of τ for an arbitrarily long orbit.

D. Example 2: The forced damped pendulum

We consider the forced damped pendulum equation,

$$\frac{d^2\phi}{dt^2} + \nu \frac{d\phi}{dt} + \Omega^2 \sin\phi = p \cos(\omega t), \quad (7)$$

for parameter values $\Omega = \omega = 1.0$, $\nu = 0.22$, and p in the vicinity of the crisis value, $p_c = 2.6465274 \dots$ (cf. also Ref. 4 for discussion of this case). In addition to describing pendula, Eq. (7) also models the dynamics of Josephson-junction circuits and of sliding charge-density waves in solids. For p slightly less than p_c there are two attractors: one with $d\phi/dt > 0$ on average and one with $d\phi/dt < 0$ on average. Given the existence of the clockwise rotating ($d\phi/dt < 0$) attractor, the existence of a counterclockwise-rotating ($d\phi/dt > 0$) attractor immediately follows from the symmetry of Eq. (7). [Equation (7) is invariant under $\phi \rightarrow -\phi$, $\omega t \rightarrow \omega t + \pi$.] Figures 8(a) and 8(b) show plots of these two attractors in the surface of section $t = 2n\pi$ (n is an integer) for $p = 2.6465 < p_c$. [The previously mentioned symmetry is not evident in Figs. 8(a) and 8(b). To see the symmetry one should examine one attractor at times $2n\pi$ and the other at time $2(n + \frac{1}{2})\pi$.] Note that each of these attractors consists of two disjoint pieces. At $p = p_c$ the two attractors simultaneously touch the stable manifolds of two unstable period-6 orbits. Following this symmetry-restoring crisis, the two chaotic attractors merge to form one single larger attractor, as illustrated in Fig. 8(c) for $p = 2.6476 > p_c$. The location of three elements of the period-6 orbit that mediate the crisis of the Fig. 8(a) attractor are shown in relation to one of the two pieces of this attractor in Fig. 8(d) (crosses denote the period-6 orbit components).

Figures 9 show time series of $d\phi/dt$ versus t for $p = 2.7 > p_c$ [Fig. 9(b) is a portion of the Fig. 9(a) orbit on a larger scale]. The intermittent switching between average clockwise and counterclockwise rotations is clearly evident. Figure 10 shows a comparison of the prediction of Eq. (3) (homoclinic case) with the data for τ from numerical experiments. Good agreement is obtained. Here τ for each value of p was computed from the surface of section time series using the technique described at the end of Sec. III C. To compute the eigenvalues β_1 and β_2 for insertion in Eq. (3) we used the technique illustrated in Fig. 3.

E. Example 3: Forced double-well duffing equation

We consider the motion of a point particle in a potential well $V(x)$ subjected to friction and an external sinusoidal force. This situation is described by the equation

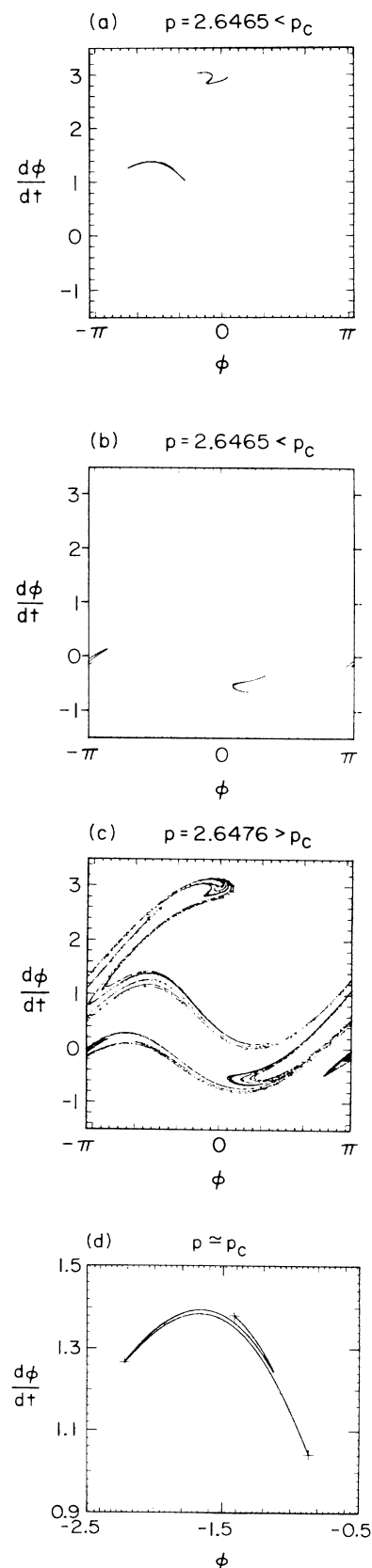


FIG. 8. Surface of section plots for the forced damped pendulum, Eq. (7).

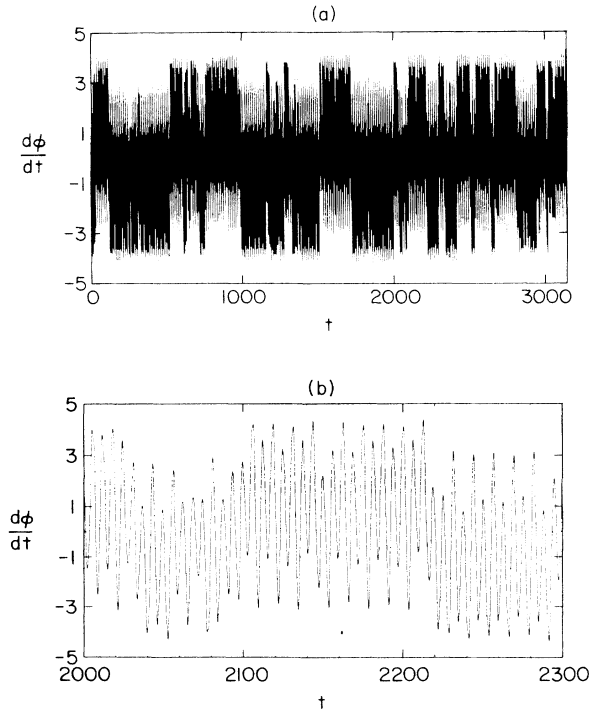


FIG. 9. Time series for the forced damped pendulum for $p = 2.7 > p_c$.

$$d^2x/dt^2 + \nu dx/dt + \partial V/\partial x = p \sin(\omega t). \quad (8)$$

We take $V = \alpha x^4/4 - \beta x^2/2$, $\nu = 1$, $\alpha = 100$, $\beta = 10$, $\omega = 3.5$, and examine Eq. (8) for p in a range about its crisis value $p_c \cong 0.849$. The potential well $V(x)$ has two minima at $x = \pm(\beta/\alpha)^{1/2}$. Just below p_c there are two symmetrically disposed chaotic attractors, one confined to the well in $x < 0$ and one confined to the well in $x > 0$. Just past $p = p_c$ there is one chaotic attractor subsuming these two $p < p_c$ attractors. The orbits for the case $p > p_c$ correspondingly represent intermittent switching between the $x > 0$ and $x < 0$ wells. Figures 11 and 12 taken from Ref. 8 by Ishii *et al.* display this behavior.

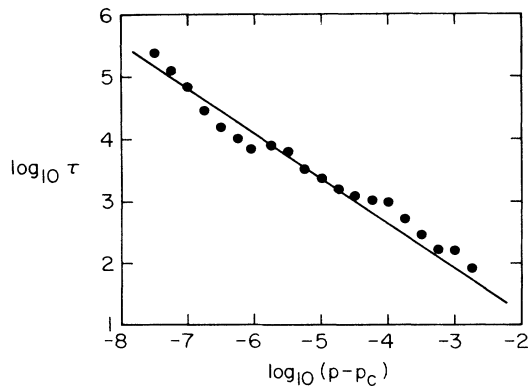


FIG. 10. Data and theoretical prediction for τ vs $(p - p_c)$ for the forced damped pendulum.

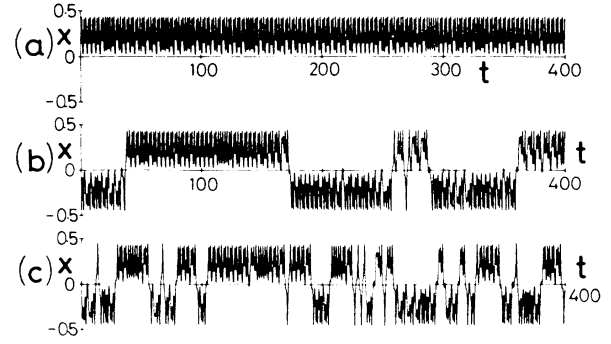


FIG. 11. Typical temporal evolutions of the particle position $x(t)$ for (a) $p < p_c$ and (b), (c) $p > p_c$. The parameter p is chosen as (a) $p = 0.849$, (b) 0.853 , and (c) 0.865 .

Examination of this case shows that at $p = p_c$ the two $p < p_c$ attractors simultaneously experience a tangency with the stable manifolds of two period-3 saddle orbits. Application of Eq. (3) then yields $\gamma = 0.703$, which, as in our previous examples, is in very good agreement with the numerical experiments.

Finally, we note that the intermittent switching in this example and in that of Sec. IID leads to distinctive characteristic features in frequency power spectra of the time series (cf. Refs. 4 and 8). This aspect will be discussed in the next example.

F. Example 4: Pairwise merging of chaotic bands in period-doubling cascades

First consider the quadratic map

$$x_{n+1} = p - x_n^2. \quad (9)$$

As shown in Fig. 13, past the point of accumulation of period-doubling bifurcations there is a successive merging of chaotic bands. Thus, for p slightly less than p_m in the figure, there are 2^m chaotic bands, while for p slightly greater than p_m there are 2^{m-1} bands. This transition is accomplished by the pairwise merging of bands at unstable orbits of period 2^{m-1} [the period 2 ($m=2$) and period 1 ($m=1$) unstable orbits are shown in the figure as the dashed and dot-dashed lines].

If we take a point in one of the 2^m chaotic bands for p slightly less than p_m , the orbit point will always return to that band after 2^m iterates. Thus that band may be

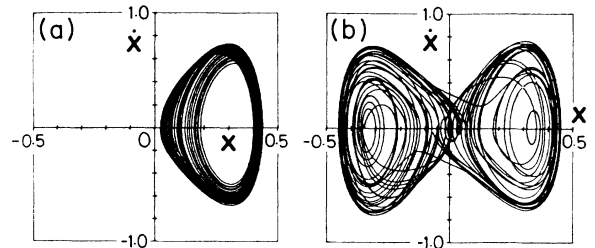


FIG. 12. Typical phase-space portraits of (8) for (a) $p = 0.8492 < p_c$ and (b) $p = 0.865 > p_c$. For $p = 0.8492$, there is another chaotic attractor in $x < 0$ statistically the same as in (a), which is realized for different initial conditions.

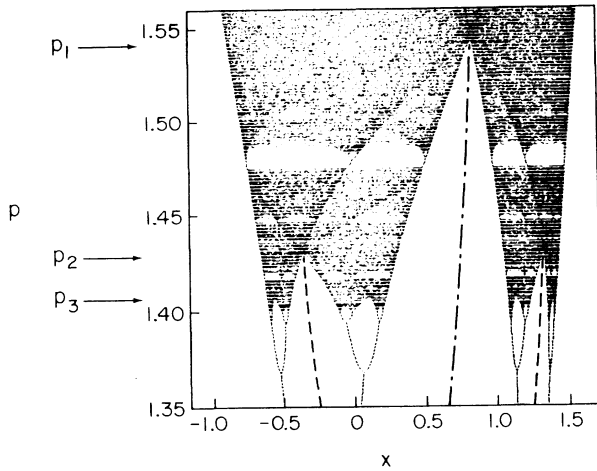


FIG. 13. Bifurcation diagram for the map $x_{n+1} = p - x_n^2$ in the range $1.35 < p < 1.56$. Within this range of p values there is an infinity of band mergings. The mergings undergo an inverse cascade and accumulate at $p_\infty = 1.4011\ldots$. We have labeled the first three consecutive band mergings by, respectively, p_1 , p_2 , and p_3 . The dashed-dotted lines indicate an unstable period-1 orbit, while the dashed lines indicate an unstable period-2 orbit.

regarded as an attractor of the 2^m -times-iterated map. Similarly, the band with which it merges at $p = p_m$ may also be regarded as an attractor of the 2^m -times-iterated map. Thus at $p = p_m$ we have what may be thought of as a simultaneous crisis of these two attractors in which they collide with the unstable period- 2^{m-1} orbit between these bands. Corresponding to this, for p slightly greater than p_m , one sees that the orbit generated by the 2^m -times-iterated map displays an occasional intermittent switching between long orbit stretches where x stays on one side (left or right) of the unstable orbit. Due to the quadratic maximum in Eq. (9), the average time between these intermittent switches scales as Eq. (1) with $\gamma = \frac{1}{2}$. This situation also has important implications for the discrete-time Fourier transform of such an orbit.^{11,12} As already mentioned, if $p_{m+1} < p < p_m$ and we take a point in one of these 2^m bands and iterate the map 2^m times, the point will come back to that band. However, if we examine the orbit every 2^m th successive iterate, we see a chaotic-looking trajectory within the band. A discrete-time Fourier transform of the orbit reflects this situation; it consists of δ -function peaks at frequencies $\omega = n\omega_m$ [with $\omega_m \equiv 2\pi(2^{-m})$ and $n = 1, 2, \dots, 2^m$] plus a continuum spectrum. (Recall that for the discrete-time Fourier transform, ω lies between 0 and 2π .) The δ functions correspond to the fact that we know with absolute certainty that an orbit in a given band will return precisely to that band 2^m iterates later, while the broadband continuum component of the spectrum reflects the chaotic motion within the bands. As p increases from below p_m to above p_m , the number of bands halves. Correspondingly, the number of δ functions must also halve. This occurs by broadening each of the components at $\omega_m, 3\omega_m, \dots, (2^m - 1)\omega_m$ into an approxi-

mately Lorentzian shape. The width of these Lorentzian components increases from zero as p is raised from p_m . As $(p - p_m)$ increases further the broadened peaks overlap and lose their individual identity. This is illustrated in Figs. 14 for $m = 2$ (this figure is taken from Ref. 11).

As shown in Refs. 11 and 12, the width of these Lorentzians scales as $\Delta\omega \sim 1/\tau$, or, from Eq. (1),

$$\Delta\omega/\omega_m \sim |p - p_m|^\gamma, \quad \gamma = \frac{1}{2}.$$

(For large m , Brown *et al.*¹¹ show that $\Delta\omega/\omega_m \cong \psi[(p - p_m)/(p_{m-1} - p_m)]^{1/2}$, where ψ is a universal number, $\psi \cong 42$.)

How is the $\gamma = \frac{1}{2}$ result for band mergings modified when we consider a two-dimensional map rather than a one-dimensional map? Figures 15 shows the attractor for the Henon map,

$$x_{n+1} = p - x_n^2 - Jy_n, \quad (10a)$$

$$y_{n+1} = x_n, \quad (10b)$$

for $J = 0.3$ and p slightly below [Fig. 15(a)], at [Fig. 15(b)], and slightly above [Fig. 15(c)] $p = p_1$. Also shown in Fig. 15 is part of the stable manifold (dashed lines) of the unstable fixed point with the two attractor pieces on either side in Fig. 15(a) [the fixed point is the large dot in Fig. 15(a)]. At $p = p_1$ [Fig. 15(b)] the attractor pieces becomes tangent to the stable manifold of the unstable period-1 fixed point orbit. We have also examined the unstable manifold of the period-1 orbit, and we find that it constitutes the outer edge of the attractor, as in Fig. 2(b). Thus the "crisis" (for the 2-times-iterated map) is of the homoclinic type, and Eq. (3) determines γ . As we look at higher and higher order band mergings, we obtain a universal correction to the one-dimensional result. In particular, we rewrite Eq. (3) for the band merging near $p = p_m$ as $\gamma \equiv \gamma_m = (\frac{1}{2}) + (\frac{1}{2})\ln\beta_1/\ln(\beta_1\beta_2)^{-1}$. For m greater than 2 or 3 we expect that β_1 is close to its value for the one-dimensional map. In fact, as $m \rightarrow \infty$, β_1 rapidly approaches a universal value for one-dimensional maps with a quadratic maximum,

$$\beta_1 \cong 1.718.$$

Furthermore, noting that $\beta_1\beta_2 = J^{2^{m-1}}$, we have

$$\gamma_m = \frac{1}{2} + \frac{\eta}{2^m} \frac{1}{\ln(1/J)}, \quad (11)$$

where the universal number η is $\eta = \ln\beta_1 \cong 0.541$, and J is the Jacobian of the map (assumed constant). Note that the one-dimensional result ($\gamma = \frac{1}{2}$) is recovered in the limit $J \rightarrow 0$.

III. ANALYSIS FOR TWO-DIMENSIONAL MAPS

In this section we derive Eqs. (2) and (3), which give the critical exponent γ in terms of eigenvalues of unstable orbits.

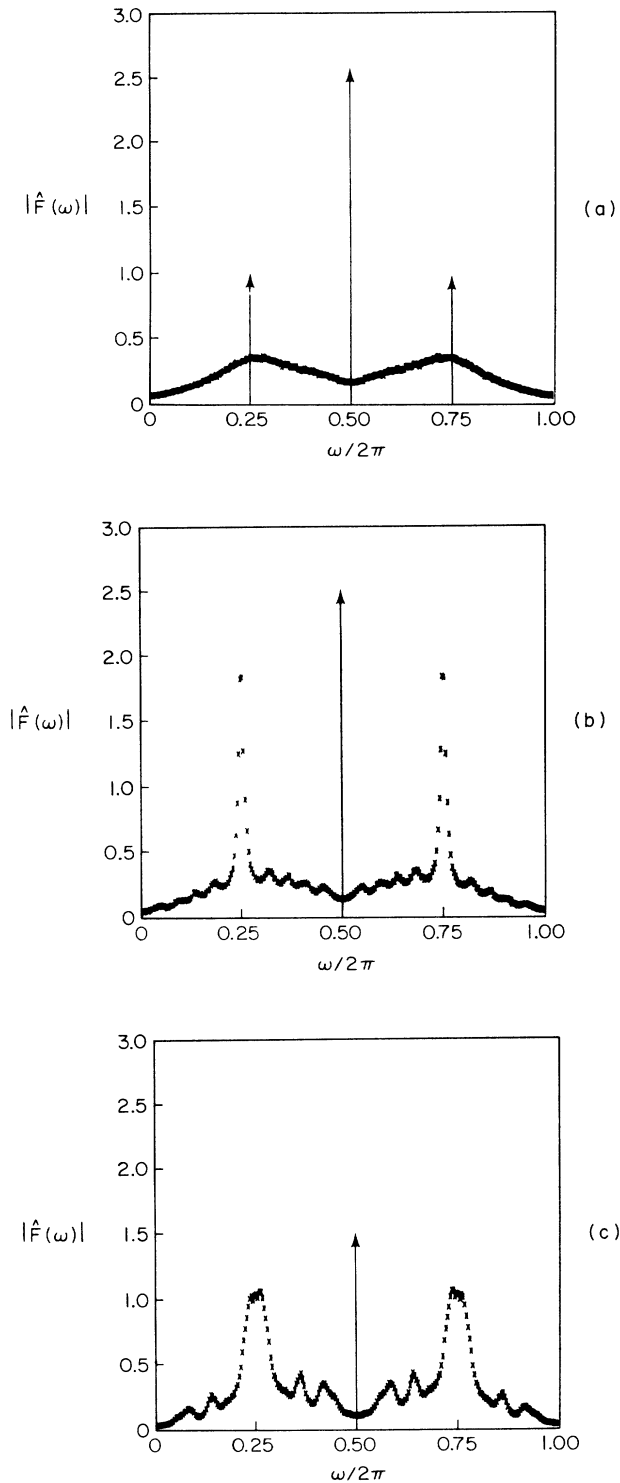


FIG. 14. (a) Smoothed Fourier transform of an orbit x_n for $p = p_2 = 1.430 \dots$. Notice the δ function peaks at $\omega/2\pi = \frac{1}{4}$, $\frac{1}{2}$, and $\frac{3}{4}$. (b) p has been increased to $(p - p_2)/(p_1 - p_2) = 0.0080 \dots$. Two of the peaks have broadened to a finite width, while the peak at $\frac{1}{2}$ is still a δ function. (c) p has increased to $(p - p_2)/(p_1 - p_2) = 0.078 \dots$.

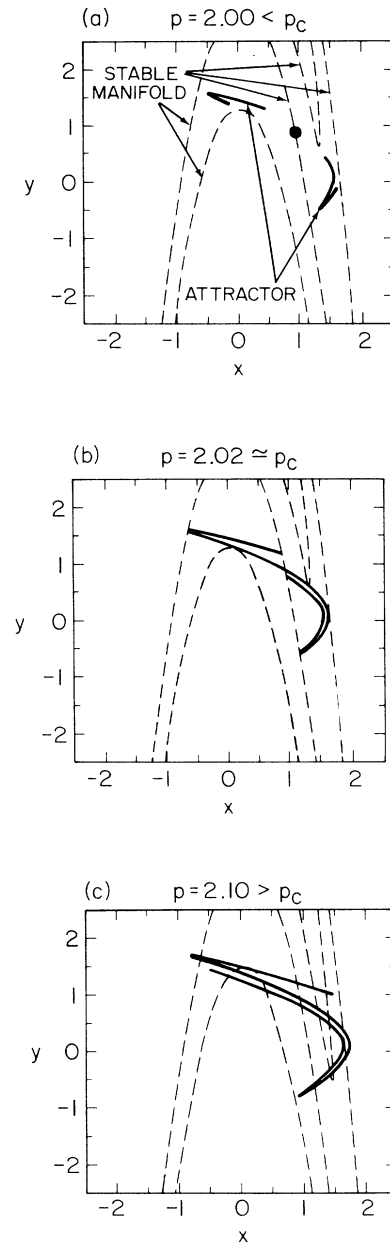


FIG. 15. Chaotic attractor of the Henon map for (a) $p = 2.00 < p_c$, (b) $p = 2.02 \approx p_c$, and (c) $p = 2.10 > p_c$.

A. Derivation of Eq. (2)

For the heteroclinic crisis, as p is increased past p_c , the unstable manifold of A crosses the stable manifold of B (cf. Fig. 16). Before the crisis the attractor was confined to the region to the right of the upper stable manifold segment of B . After the crisis an orbit initially in the region in which the chaotic attractor was confined for $p < p_c$ can eventually land in the cross-hatched region ab of Fig. 16. Such an orbit will then be attracted along the stable manifold of B and then rapidly leave the

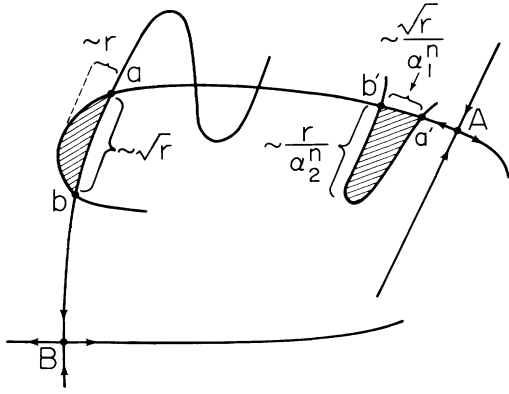


FIG. 16. Schematic diagram illustrating the derivation of Eq. (2).

region to which the chaotic attractor was confined for $p < p_c$, moving to the left along the outward (left-going) branch of the unstable manifold of B . For p near p_c , the dimensions of region ab are of the order r and $r^{1/2}$, where $r = p - p_c$ (cf. Fig. 16). We now iterate the region ab backwards in time for n steps. For large-enough n , except for the first few backwards iterates, the change in the region ab is governed by the linearization of the map about A . Thus the preiterated region $a'b'$ has dimensions of the order of r/α_2^n and $r^{1/2}/\alpha_1^n$, as shown in Fig. 16. Since after falling in region $a'b'$ the orbit soon (i.e., n steps after) falls in region ab , we estimate τ as the average time it takes an orbit to land in region $a'b'$. Now consider the probability measure of the attractor at $p = p_c$. τ^{-1} is then estimated as the probability that an orbit on the $p = p_c$ attractor falls on a given iterate in the region $a'b'$, and we denote this probability by $\mu(r)$. Now reduce r by the factor $\alpha_2(r \rightarrow \alpha_2 r)$ and consider the resulting region ab . After we iterate backwards $n+1$ steps (instead of n), the long dimension of the preiterated region is again r/α_2^n but the width is changed to $(\alpha_2 r)^{1/2}/\alpha_1^{n+1}$. Assuming that, for our purposes, the attractor measure can be treated as if it were smooth in the direction of the unstable manifold of A , we have

$$\frac{\mu(r)}{\mu(\alpha_2 r)} \sim \frac{r^{1/2}/\alpha_1^n}{(\alpha_2 r)^{1/2}/\alpha_1^{n+1}} = \frac{\alpha_1}{\alpha_2^{1/2}}.$$

With the assumption that $\mu(r) \sim r^\gamma$, Eq. (2) then follows.¹³

B. Derivation of Eq. (3)

Consider the situation at $p = p_c$ represented schematically in Fig. 17. We denote the measure of the attractor in the shaded region defined by the unstable manifold segment aoc and the vertical line abc by $\mu(\epsilon)$, where we take the vertical line abc to be a distance ϵ from the stable manifold of B . We assume that $\mu(\epsilon) \sim \epsilon^\gamma$, for small ϵ , and, as in Sec. III A, we identify the exponent for $\mu(\epsilon)$ with that governing the scaling of the characteristic time $\tau(\tau \sim |p - p_c|^{-\gamma})$. The basis for this assumption is that, for $r = p - p_c$ positive and small, we ex-

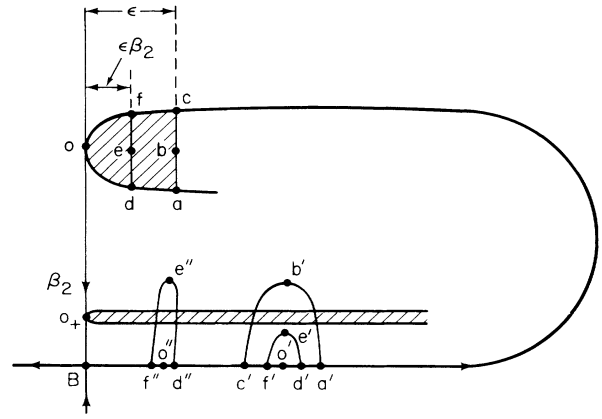


FIG. 17. Schematic illustrating derivation of Eq. (3).

pect the unstable manifold of B shown to poke over to the other side of the stable manifold by a distance of order r (as in Fig. 16). Thus taking $\epsilon \sim r$ we have $\tau^{-1} \sim \mu(\epsilon)$.

Also shown in Fig. 17 is a second vertical line segment def which has been chosen a distance $\epsilon\beta_2$ from the stable manifold of B . The measure of the attractor in the region $defod$ is $\mu(\epsilon\beta_2)$. Our goal in what follows will be to estimate the ratio $\mu(\epsilon\beta_2)/\mu(\epsilon)$. By doing this we shall be able to determine the exponent γ .

Imagine that we iterate the cross-hatched region backwards in time many iterates so that the points (a, b, c, d, e, f, o) map to $(a', b', c', d', e', f', o')$ which are close to B (for ϵ small). Now iterate the region $d'e'f'o'd'$ backward one further iterate to $d''e''f''o''d''$. Since the primed letters are close to B , this one further backward iterate is governed by the linearized map at B (i.e., by the eigenvalues β_1 and β_2 evaluated at B). Thus the distance from o' to e' is stretched by β_2^{-1} to $o''e''$, while the segment $f'o'd'$ is compressed by β_1^{-1} to become the shorter segment $f''o''d''$. Note, however, that, since the original distance from o to e (namely, $\epsilon\beta_2$) was chosen to be shorter by precisely the factor β_2 than the distance from o to b (namely, ϵ), we now have that the distance from e'' to o'' is the same as that from b' to o' . Also, since the tangency of the stable and unstable manifolds at o is quadratic, we have that the curve segment fod is shorter than the curve segment coa by $\sqrt{\beta_2}$. Since ϵ is small, this also implies that the segment $f'o'd'$ is shorter than $c'o'a'$ by $\sqrt{\beta_2}$. Putting these facts together we summarize the relevant information as follows:

$$\overline{(o'b')} = \overline{(o''e'')}, \quad (12)$$

$$\overline{(c'o'a')} = \overline{(f''o''d'')}(\beta_1/\sqrt{\beta_2}), \quad (13)$$

where we have used a superscripted bar to denote the length of a line segment.

We now wish to obtain an estimate of the ratio of the measure of the attractor contained in the region $d''o''f''e''d''$ to the measure of the attractor contained in the region $a'o'c'b'a'$. To do this, imagine iterating

the cross-hatched region at the tangency o forward many iterates in time so that o maps to the point o_+ in Fig. 17. The cross-hatched region has now been greatly stretched out along the direction of the unstable manifold of B . Since $d\mu(\epsilon)/d\epsilon \sim \epsilon^{\gamma-1}$, we conclude that the amount of attractor measure per unit horizontal length contained in the cross-hatched region emanating from o_+ is larger in $d''o''f''e''d''$ than in $a'o'c'b'a'$ by the factor $\beta_1^{1-\gamma}$. The same result applies for other iterates of the cross-hatched region. Thus using Eq. (13) we obtain

$$\frac{(\text{measure in } d''o''f''e''d'')}{(\text{measure in } a'o'c'b'a')} = \frac{\beta_2^{1/2}}{\beta_1} \beta_1^{1-\gamma}. \quad (14)$$

Since the region $d''o''f''e''d''$ maps to $dofed$, the measure of the attractor inside $d''o''f''e''d''$ is just $\mu(\epsilon\beta_2)$. Similarly, the measure of the attractor inside $a'o'c'b'a'$ is $\mu(\epsilon)$. Thus, since $\mu(\epsilon) \sim \epsilon^\gamma$, we also have

$$\frac{(\text{measure in } d''o''f''e''d'')}{(\text{measure in } a'o'c'b'a')} = \beta_2^\gamma. \quad (15)$$

Combining Eqs. (14) and (15) we have

$$\beta_2^{1/2} = (\beta_1\beta_2)^\gamma,$$

which yields the desired result, Eq. (3) for γ .

IV. OTHER SITUATIONS

A. Higher-dimensional cases

The formulas Eqs. (2) and (3) apply only to situations described by two-dimensional maps. In higher-dimensional situations there is probably a much greater variety of ways in which crises can occur. In order to obtain some insight into the higher-dimensional situation, in this section we shall consider a particular situation and derive an expression for the exponent γ . The particular situation we consider leads to a generalization of Eq. (2). In particular, we consider a smooth D -dimensional map, and we assume that there is an attractor containing an unstable periodic orbit A which has $D-1$ unstable directions with eigenvalues $\alpha_1, \alpha_2, \dots, \alpha_{D-1}$ and one stable direction with eigenvalue α_D ($|\alpha_i| > 1$ for $i < D$ and $|\alpha_D| < 1$). We assume that the outer edge of the attractor takes the form of a smooth $D-1$ dimensional surface through A , and that the crisis occurs when this surface pokes through the basin boundary as $r = p - p_c$ increases through zero. The situation is illustrated in Fig. 18 for the case of a three-dimensional map ($D=3$). The downward icicle-shaped object near A is an n th preiterate of the shaded volume poking through the basin boundary. (Note the similarity with Fig. 16.) Proceeding as in Sec. III A we obtain the following formula for γ :

$$\gamma = (D-1)/2 + (\ln |\alpha_1\alpha_2 \cdots \alpha_{D-1}|) / |\ln |\alpha_D||. \quad (16)$$

In particular, for strictly dissipative systems (magnitude of the Jacobian determinant < 1 everywhere) we note that

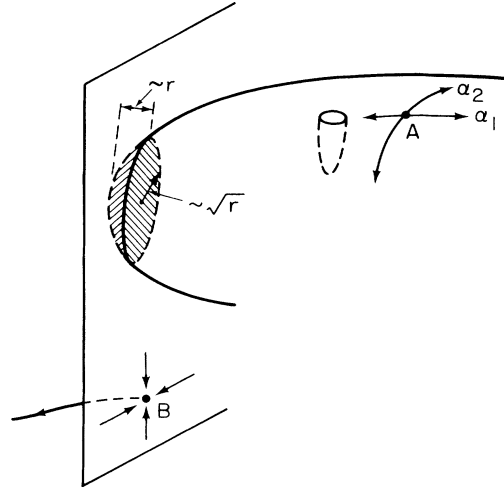


FIG. 18. Schematic for the derivation of Eq. (16).

$$(D+1)/2 \geq \gamma \geq (D-1)/2.$$

We believe that this may indicate a general tendency for γ to be larger when higher-dimensional attractors suffer crises. As discussed in Sec. I, larger values of γ correspond to long chaotic transients which tend to persist over larger parameter ranges. Thus we believe that chaotic transients may be a pervasive feature when higher-dimensional dynamical behavior is involved. Indeed this is observed to be so in experiments.¹⁴

B. The effect of fixed points in three-dimensional flows

Poincaré surfaces of section derived from systems of three coupled autonomous first-order ordinary differential equations generally yield crises described by Eqs. (2) and (3), if the equations are sufficiently smooth and the time intervals between successive piercings of the surface of section have a finite upper bound. Equations (2) and (3) may not apply, however, in many cases for which there is an unstable time-independent equilibrium solution 0 of the equations. Assume that the orbit through some point P_0 in the surface of section A_0 (cf. Fig. 19) goes exactly to 0 . Thus, for P_0 , the return time to the Poincaré surface is infinite, and, for points in the surface of section close to P_0 , the return time can be arbitrarily large. A prominent example where this occurs is the Lorenz system. In particular, in a certain parameter range there are three attractors: one is a chaotic attractor, while the other two are fixed point attractors (which are symmetrically placed in accord with the underlying symmetry of the Lorenz system). As the parameter is changed, the chaotic attractor collides with the basic boundary of the fixed-point attractors and results in a chaotic transient. Figure 19 schematically shows the situation for the case where the parameter value p is close to the crisis value p_c and there is a chaotic transient. In Fig. 19 the two fixed-point attrac-

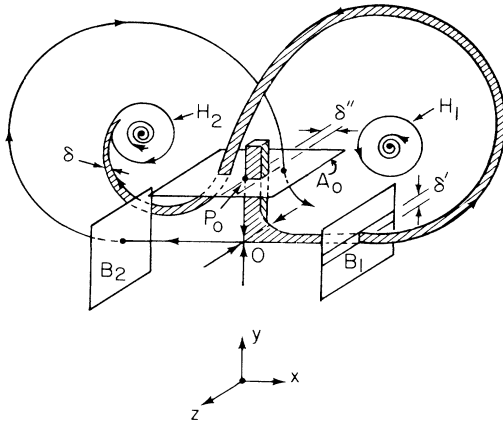


FIG. 19. Schematic for the situation for the Lorenz system for p slightly beyond p_c .

tors are encircled by unstable limit cycles H_1 and H_2 . The basins of attraction for these fixed points before the crisis (i.e., when the chaotic attractor exists) are the stable manifolds of H_1 and H_2 (not drawn), which are tubularlike regions. At $p = p_c$ the "edge of the chaotic attractor" touches these tubular regions. The edge of the attractor is defined by the unstable manifold of the fixed point 0 in the figure. Near this edge the attractor is very thin and knifelike; that is, the edge is very sharp. In order to see that this is so, consider an orbit passing through the plane A_0 close to the vertical-going stable manifold of 0. Near 0 the flow is approximated by

$$dx/dt = \alpha x, \quad dy/dt = -\beta_1 y, \quad dz/dt = -\beta_2 z, \quad (17)$$

with $\alpha, \beta_{1,2} > 0$. Because points passing near 0 spend a long time there, the equation $dz/dt = -\beta_2 z$ has a long time to act, and the z coordinate thus becomes very small. Now say $r = p - p_c$ is increased slightly from zero so that the chaotic attractor is destroyed. The unstable manifold of 0 will now intersect the stable manifolds of H_1 and H_2 . Thus, as shown in the figure, a region of width δ from the knife edge is "skimmed off" by the fixed-point attractors. Generically δ will vary linearly with $p - p_c$,

$$\delta \sim |p - p_c|.$$

In addition, if we consider the plane B_1 in Fig. 19, the width of the intersection with B_1 of the skimmed-off region will vary linearly with δ , $\delta' \sim \delta$. Taking the planes B_1 and A_0 to be close to 0, the map from B_1 to A is governed by the linear equations, Eqs. (17). Consequently we have

$$\delta'' \sim (\delta')^{\alpha/\beta_1} \sim |p - p_c|^{\alpha/\beta_1}.$$

Assuming that the probability of an orbit point crossing A_0 falls in the strip δ'' is proportional to δ'' , we have that $\tau^{-1} \sim \delta''$ or

$$\tau \sim |p - p_c|^{-\gamma},$$

with the exponent γ given by

$$\gamma = \alpha/\beta_1. \quad (18)$$

This result for the exponent γ was stated without derivation by Yorke and Yorke,¹⁵ who also carry out numerical experiments on the Lorenz equations which are consistent with (18). We reiterate that Eqs. (2) and (3) do not apply here because of the fixed equilibrium point in the flow.

ACKNOWLEDGMENT

This work was supported by the U.S. Department of Energy, Office of Basic Energy Sciences (Applied Mathematics Program).

APPENDIX: EQUALITY OF THE PERIODS OF THE PERIODIC ORBITS, A AND B , IN FIG. 2(a)

Figure 20 shows the orbits A and B at $p = p_c$. We limit consideration here to the case where the closure of the stable manifold of B is also the boundary of the basin of attraction for the attractor for $p < p_c$. In addition, we assume that the basin boundary and the basin itself are connected sets (thus the basin has no holes). A tangency of the stable manifold of B with the unstable manifold of A is labeled 0 in Fig. 20. We assume that the map is invertible and orientation preserving (i.e., its Jacobian is positive). Successive inverse images of 0 are labeled, $-1, -2, -3, \dots, -n, \dots$. These images limit on A as $n \rightarrow \infty$. Since these image points are on the basin boundary and since any boundary is a closed set, the periodic orbit A is thus on the boundary (as well as being on the attractor).

We now wish to show that any two accessible periodic orbits on the basin boundary must have the same period. Here by accessible we mean that one can construct a finite-length curve from a point in the interior of the basin to an accessible point without the curve ever crossing the basin boundary.¹⁶ The elements of the periodic

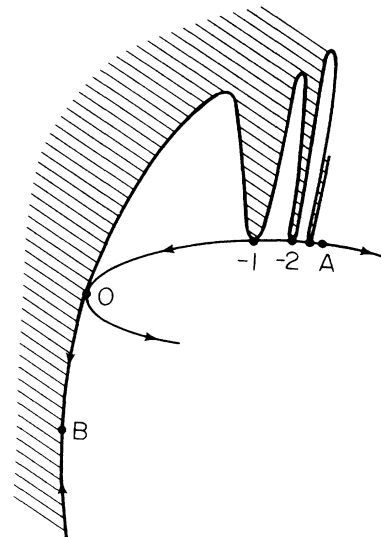


FIG. 20. The tangency points 0, $-1, -2, \dots$, limit on A .

orbits A and B are clearly accessible. Denote the elements of A by $a_i (i=1, 2, \dots; a_1=a_{q+1})$ and the elements of B by $b_i (i=1, 2, \dots; b_1=b_{r+1})$, where q and r are the periods of A and B . Let Z be an interior point of the basin and construct curves in the basin which do not cross each other and connect Z to the points a_i and b_i (cf. Fig. 21). By means of these curves the points a_i and b_i can be rotationally ordered. For example, for the case in the figure, using a clockwise reference about Z , we have the ordering $\dots b_r, a_1, b_1, a_2, \dots$. Now apply the map to the points Z , a_i and b_i and to the curves connected with Z . Under the map $Z \rightarrow Z'$, where Z' is in the interior of the basin, and the original curves from Z map to new curves connecting Z' to the a_i and b_i . Since the map is invertible, the new curves do not cross each other. Since the map is presumed to have positive Jacobian, it preserves orientation. Thus the rotational ordering of points on the boundary is invariant under application of the map. Now consider two elements (consecutive in terms of the clockwise ordering) of A denoted a_j and a_{j+1} . Say that in the rotational ordering a_j and a_{j+1} have p elements of B between them. That is, the ordering is $a_j, b_m, b_{m+1}, \dots, b_{m+p-1}, a_{j+1}$. (We choose j so that there is at least one element of B between a_j and a_{j+1} , i.e., $p \neq 0$.) Now apply the map q times to these points. Since q is the period of A , a_j and a_{j+1} are mapped back to each other. Since, however, ordering is preserved, each of the $b_m, b_{m+1}, \dots, b_{m+p}$ must also be mapped back to itself. Hence the periods q and r must be equal. [It follows that between each pair of consecu-

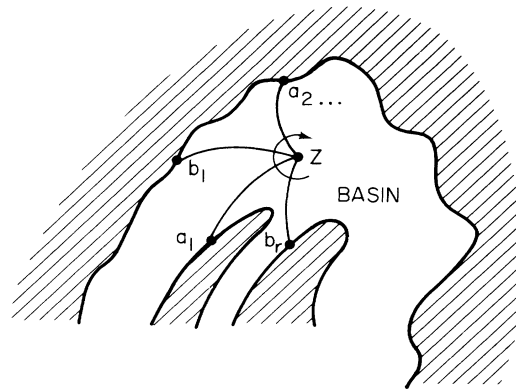


FIG. 21. Schematic of basin and accessible periodic points on the boundary. The region outside the basin is shown cross hatched.

tive elements of A there must be exactly one element of B (i.e., p is one.)]

While the above arguments have been for the case where the closure of the stable manifold of B is the basin boundary, we believe that these arguments can be extended to the case where the stable manifold of B lies in the basin of the attractor (an "interior crisis," cf. Refs. 1 and 2). Finally, for the negative Jacobian case, consideration of the second iterate of the map (which has positive Jacobian) shows that either $q=r$, or, if not, then q or r is one and the other is two.

*Present address: Centro de Eletrodinâmica, Instituto Superior Técnico, 1096 Lisbon Codex, Portugal.

¹C. Grebogi, E. Ott, and J. A. Yorke, Phys. Rev. Lett. **48**, 1507 (1982).

²C. Grebogi, E. Ott, and J. A. Yorke, Physica (Amsterdam) **7D**, 181 (1983).

³For example, C. Jeffries and J. Perez, Phys. Rev. A **27**, 601 (1983); S. D. Brorson, D. Dewey, and P. S. Lindsay, Phys. Rev. A **28**, 1201 (1983); H. Ikezi, J. S. DeGrasse, and T. H. Jensen, Phys. Rev. A **28**, 1207 (1983); M. Iansiti, Q. Hu, R. M. Westervelt, and M. Tinkham, Phys. Rev. Lett. **55**, 746 (1985); D. Dangoisse, P. Glorieux, and D. Hannequin, Phys. Rev. Lett. **57**, 2657 (1986).

⁴E. G. Gwinn and R. M. Westervelt, Phys. Rev. A **33**, 4143 (1986).

⁵Several examples of crisis induced intermittency are the following: J. Maurer and A. Libchaber, J. Phys. Lett. **41**, L515 (1980); D. D'Humieres, M. R. Beasley, B. A. Huberman, and A. Libchaber, Phys. Rev. A **26**, 3483 (1982); M. Kitano, T. Yabuzaki, and T. Ogawa, *ibid.* **29**, 1288 (1984); R. W. Rollins and E. R. Hunt, *ibid.* **29**, 3327 (1984); Y. Yamaguchi and H. Minowa, *ibid.* **32**, 3758 (1985); H. Fujisaka, H. Kamikimoto, and M. Inoue, Progr. Theor. Phys. **69**, 333 (1983); Y. Gu, M.-W. Tung, J.-M. Yuan, D. H. Feng, and L. Narducci, Phys. Rev. Lett. **52**, 701 (1984); O. Sporns, S. Roth, and F. F. Seelig, Physica **26D**, 215 (1987); R. M. Everson, Phys. Lett. **122A**, 471 (1987).

⁶Y. Pomeau and P. Manneville, Commun. Math. Phys. **74**, 189 (1980).

⁷C. Grebogi, E. Ott, and J. A. Yorke, Phys. Rev. Lett. **57**, 1284 (1986).

⁸H. Ishii, H. Fujisaka, and M. Inoue, Phys. Lett. **116A**, 257 (1986).

⁹C. Grebogi, E. Ott, and J. A. Yorke, Phys. Rev. Lett. **50**, 935 (1983); Ergod. Theor. Dynam. Sys. **5**, 341 (1985).

¹⁰J. A. Yorke, DYNAMICS, a program for IBM PC clones for interactive study of dynamics.

¹¹R. Brown, C. Grebogi, and E. Ott, Phys. Rev. A **34**, 2248 (1986).

¹²S. J. Shenker and L. P. Kadanoff, J. Phys. A **14**, L23 (1980); A. S. Pikovsky, Radiophys. **29**, 1438 (1986).

¹³In obtaining an estimate for $\mu(r)$, one might be tempted to use the scaling which follows from application of the pointwise dimension equated to the Lyapunov-number formula for the information dimension of the chaotic attractor [cf. J. D. Farmer, E. Ott, and J. A. Yorke, Physica **7D**, 153 (1983)]. The result would be Eq. (2) but with α_1 and α_2 incorrectly replaced by the Lyapunov numbers of the attractor. The resolution of this apparent disagreement is that the pointwise dimension is equal to the attractor's information dimension for *almost all* points with respect to the attractor measure. However, points on the outer edge of the attractor are exceptional in that they are part of the measure zero set for which the pointwise and information dimensions are not

equal.

- ¹⁴G. Ahlers and R. W. Walden, Phys. Rev. Lett. **44**, 445 (1980); J. P. Gollub and J. F. Steinman, *ibid.* **47**, 505 (1981); P. Bergé and M. Dubois, Phys. Lett. **93A**, 365 (1983); T. L. Carroll, L. M. Pecora, and F. J. Rachford (unpublished); A. Libchaber (private communication).

- ¹⁵J. A. Yorke and E. D. Yorke, J. Stat. Phys. **21**, 263 (1979).

- ¹⁶For a smooth, nonfractal basin boundary all boundary points are accessible from the basin. For fractal basin boundaries of dissipative invertible two-dimensional maps the boundary

points accessible from the basin are a relatively small subset of all the basin boundary points in the following sense: A line intersecting the basin boundary typically contains a countable infinity of accessible boundary points and an uncountable infinity of inaccessible boundary points [C. Grebogi, E. Ott, and J. A. Yorke, Phys. Rev. Lett. **56**, 1011 (1986); Physica **25D**, 243 (1987)]. There are commonly an infinite number of inaccessible periodic orbits with different periods in a fractal basin boundary.